Article

Journal of
Biomedical Nanotechnology
Vol. 16, 1–11, 2020
www.aspbs.com/jbn

Facile Ultrasound-Triggered Release of Calcein and Doxorubicin from Iron-Based Metal-Organic Frameworks

Mihad Ibrahim[1], Rana Sabouni[1], Ghaleb A. Husseini[1,*], Abdollah Karami[1], Reenu Geetha Bai[2], and Debasmita Mukhopadhyay[1]

[1] *Department of Chemical Engineering, American University of Sharjah, Sharjah, United Arab Emirates*
[2] *School of Natural Sciences and Health, Tallinn University, Narva mnt 29, 10120 Tallinn, Estonia*

Metal-organic frameworks (MOFs) are promising new nanocarriers with potential use in anticancer drug delivery. However, there is a scarcity of studies on the uptake and release of guest molecules associated with MOF nanovehicles, and their mechanism is poorly understood. In this work, newly developed iron-based MOFs, namely Fe-NDC nanorods, were investigated as potential nanocarriers for calcein (as a model drug/dye) and Doxorubicin (a chemotherapeutic drug (DOX)). Calcein was successfully loaded by equilibrating its solution with the MOFs nanoparticles under constant stirring. The calcein average encapsulation efficiency achieved was 43.13%, with a corresponding capacity of 17.74 wt.%. *In-vitro* calcein release was then carried out at 37 °C in phosphate buffer saline (PBS) using ultrasound (US) as an external trigger. MOFs released an average of 17.8% (without US), whereas they released up to 95.2% of their contents when 40-kHz US at ~1 W/cm^2 was applied for 10 min. The ~~cytostatic~~ drug DOX was also encapsulated in Fe-NDC, and its *In-vitro* release profile was determined under the same conditions. DOX encapsulation efficiency and capacity were found to be 16.10% and 13.37 wt.%, respectively. *In-vitro* release experiments demonstrated significant release, reaching 80% in 245 minutes, under acoustic irradiation, compared to around 6% in the absence of US. Additionally, experimental results showed that Fe-NDC nanoparticles are biocompatible even at relatively high concentrations, with an MCF-7 IC_{50} of 1022 μg/ml. Our work provides a promising platform for anticancer drug delivery by utilizing biocompatible Fe-NDC nanoparticles and US as an external trigger mechanism.

KEYWORDS: *Metal-Organic Frameworks (MOFs), Encapsulation, Calcein, Doxorubicin, Ultrasound, Biocompatibility.*

INTRODUCTION

Over the past few decades, the encapsulation of antineoplastic agents in nanocarriers has been extensively studied to reduce the side effects of conventional chemotherapy [1–6]. These nanovehicles are characterized by small size, low cytotoxicity, biocompatibility, and an ability to entrap high concentrations of therapeutic agents. Additionally, they can be detected by imaging techniques [7–9].

The fenestrations found in the defective blood microvessels and the poor lymphatic drainage in tumors are behind the enhanced permeability and retention (EPR) phenomenon. This phenomenon is utilized to design various targeted nanoparticle-based anti-tumor therapies [10–12]. The EPR effect was first reported in 1986 by Maeda and coworkers when they discovered that large molecules (with a molecular weight higher than 40–50 kDa) accumulate in cancer tissues for extended durations compared to healthy tissues [5, 10, 13].

Most tumors have microvessels with a vascular pore cutoff size ranging between 380 and 800 nm [14, 15] depending on the tumor location, type, and environment [16]. Nanomaterials used to sequester and deliver anticancer drugs are divided into two broad categories: organic (liposomes, micelles, dendrimers, etc.) and inorganic (mesoporous silica, carbon nanotubes, zeolites, etc.) [17–19].

Recently, a new type of porous material, namely Metal-Organic Frameworks (MOFs), has emerged and attracted considerable attention as possible promising nanocarriers for drug delivery applications. MOFs are self-assembled hybrid materials of inorganic clusters (metal salts) with organic compounds (bridging linkers) that form network arrangements with well-defined crystallinity and high porosity [7, 20–23]. Given the facile coordination of their

*Author to whom correspondence should be addressed.
Email: ghusseini@aus.edu
Received: 21 September 2020
Accepted: 9 November 2020

organic and inorganic parts, MOFs help address the shortcomings of inorganic nanocarriers (limited biocompatibility and biodegradability) and organic nanocarriers (low stability).

Several research groups first investigated the use of MOFs as smart drug carriers, including the encapsulation of ibuprofen in MIL (Materials of Institute Lavoisier)-100 and MIL-53, busulfan in MIL-89, MIL-88A, MIL-100 and MIL-53, and DOX and topotecan in MIL-100 [24–28]. More recently, several MOFs drug delivery systems (DDSs) were studied for the encapsulation of camptothecin, DOX and 5-fluorouracil in ZIF-8, mitoxantrone and [Ru(p-cymene)Cl_2(pta)] (RAPTA-C) in ZnBDP_X series, DOX in Gd-pDBI and MG-Gd-pDBI, etc. [29–33].

The presence of organic and inorganic groups, their tunable porosity, high crystallinity, and the possibility of functionalizing their external and internal surface enhances MOFs potential use in drug delivery. Other desirable MOFs' characteristics include their biocompatibility and their ability to encapsulate high payloads of chemotherapeutic drugs [7, 20, 21, 24].

Ultrasound (US) is currently being researched as a modality to trigger drug release from nanoemulsions, micelles, liposomes, and polymeric nanoparticles [34–38]. This technique effectively enhances drug delivery from nanocarriers and transport into the cytosol of tumor cells. Two potential effects of acoustically activated drug delivery could be at play, i.e., thermal and nonthermal [35, 39–41]. Thermal effects include the interaction between US and biological tissues due to a localized temperature increase caused by energy absorption. Nonthermal effects are caused by mechanical and cavitation effects. The motion of the fluid causes mechanical forces in the vicinity of the nanocarrier via pressure waves and acoustic streaming, both of which can increase drug transport into the cells. Cavitation is defined as the formation and oscillation of tiny gas bubbles (microbubbles) in tissues due to US-induced vibrations. This generates high stresses on cell membranes and nanocarriers, resulting in the possible collapse of these bubbles, and the subsequent release of the encapsulated agent [34, 36, 42].

Existing diagnostic and therapeutic applications of US, such as sonophoresis (transdermal drug delivery), blood clots disruption, kidney stone breakage, fat cavitation (body contouring), and eye surgeries (cataract removal), have demonstrated the safety and biotolerance of such technology [43–48]. Other studies have reported on the safety and bioeffects of US in various medical applications [49–52].

This study describes the first application of our previously synthesized and characterized MOFs [53], namely Fe-NDC nanorods, as nanoparticles for delivering antineoplastic agents. The novelty of the present work lies in its (1) ease of encapsulation and (2) the use of noninvasive US waves to trigger release. *To the best of our knowledge, this is the first report of using acoustic power to release encapsulated DOX from MOFs*. In addition to encapsulating DOX, the synthesized MOFs were loaded with a model drug/dye, i.e., calcein. *In-vitro* release profiles were studied in phosphate buffer saline (PBS) at 37 °C with (and without) low-frequency low-intensity US. We also examined the biocompatibility of Fe-NDC nanoparticles using flow cytometry and MCF-7 cells.

EXPERIMENTAL DETAILS

Materials

All chemicals required to prepare Fe-NDC were purchased from Sigma–Aldrich (through their supplier LABCO, Dubai, United Arab Emirates) and used as received. The chemicals used were iron nitrate nonahydrate ($Fe(NO_3)_3 \cdot 9H_2O$, ACS reagent, ≥98%), 2,6-Naphthalenedicarboxylic acid (2,6-NDC, 95%), and *N*, *N*-dimethylformamide (DMF, ReagentPlus®, ≥99%), and methanol (Puriss., Ph Eur, ≥99.7% (GC grade)). To culture cells and investigate the cytotoxicity of MOFs, fetal bovine serum (FBS), penicillin–streptomycin, trypsin (0.25%), and propidium iodide were used, also purchased from LABCO (Dubai, United Arab Emirates). Calcein disodium salt was purchased from Honeywell Fluka™ (Charlotte, North Carolina, USA) and Doxorubicin (DOX) was obtained from Euroasia Trans Continental (Mumbai, India).

Synthesis and Characterization of Fe-NDC

The MOF (Fe-NDC) was synthesized according to the procedure described previously by Ibrahim et al. [53]. Typically, 0.0932 g of $Fe(NO_3)_3 \cdot 9H_2O$, and 0.0499 g of 2,6-NDC were mixed and dissolved in 10 ml of DMF. The precursor solution was transferred to a 23-ml microwave acid digestion vessel and heated via microwave irradiation at 160 W for 5 min. The resultant synthesized brown particles were collected by centrifugation (4500 rpm, 1 hour) using a benchtop centrifuge (Heraeus Megafuge 8R, Thermo Scientific, Waltham, MA, USA), washed twice with DMF to remove the unreacted precursor and DMF from the pores of the material. Finally, the washed Fe-NDC particles were dried in an oven at 100 °C. The synthesized MOF samples were characterized using several characterization tests, including X-ray diffraction (XRD), scanning electron microscopy (SEM), and Brunauer–Emmett–Teller (BET) surface area analysis. The XRD patterns were obtained using the Bruker D8 Advance equipment at room temperature using a Cu Ka ($\lambda = 1.54$ Å) radiation source on a silicon wafer from 3 to 40° (2θ) with a step size of 0.02° and 1 s (per step) in a continuous mode. The morphology and microscopic structure were studied using SEM by MIRA3 XMU (Tescan Orsay Holding, Czech Republic) after coating the MOF samples with gold. Additionally, the pore-filling mechanism was investigated cryogenically via nitrogen gas physisorption isotherms using a TriStar II

3020 Micromeritics instrument at 77.350 K (liquid nitrogen temperature). The volumetric adsorbed amounts of gas (cm^3/g) were measured as a function of the relative pressure (p/p° = absolute/saturation pressure). The particle size distribution, average particle diameter, and polydispersity index (PDI) of Fe-NDC were determined using a dynamic light scattering instrument (DynaPro NanoStar, Wyatt Technology, Santa Barbara, CA, USA) as follows: Initially, Fe-NDC samples were added to a PBS solution to achieve a concentration of approximately 7 μg/ml, and sonicated for 10 minutes. Then, around 60 μl of the suspension was transferred to a cuvette and placed inside the instrument at room temperature. The results were averaged over 10 acquisitions. The details of other characterization tests (Fourier transform infrared spectroscopy, energy-dispersive X-ray, thermogravimetric analysis, and pore volume analysis) are available in our previously published paper [53].

Calibration Curve of Calcein Disodium Salt and DOX

Because of its low cost, calcein and its salt are extensively used as dyes to study the behavior of anticancer agents [54–57]. Therefore, in this study, we first investigated the loading and release of calcein under US irradiation to understand its mechanism. Then, we extend the US-triggered release to DOX.

Different neutral solutions of calcein in PBS were prepared with concentrations of 0.0015, 0.0025, 0.0075, 0.005, 0.01, 0.015, 0.02, and 0.025 mM. The absorbance of the prepared solutions was measured using an Evolution™ 60S UV-visible spectrophotometer (Thermo Scientific, Waltham, MA, USA) between 400–550 nm. Then, the calibration curve was generated using the concentrations of the standard solutions. Similarly, standard DOX solutions were prepared in PBS at different concentrations (0.0156–0.25 mM) and their UV-visible spectra were measured to generate the DOX calibration curve.

Calcein Disodium Salt Encapsulation Experiments

Encapsulation was achieved via the simple impregnation method. First, calcein disodium salt was dissolved in a mixture of pure methanol and a 1-M aqueous NaOH solution (a methanol: NaOH ratio of 5:1) to obtain a final calcein concentration of 5 mg/ml. Then, 100 mg of Fe-NDC nanoparticles were added to 10 ml of the calcein solution at room temperature under magnetic stirring in the dark for two days. The resulting suspension was centrifuged (4500 rpm, 1 hour, Heraeus Megafuge 8R, Thermo Scientific, Waltham, MA, USA), and the supernatant was decanted carefully. The loaded nanorods were washed twice with deionized water and then collected and dried.

In order to determine the amount of calcein disodium salt encapsulated inside the porous matrices after each experiment, aliquots from the supernatant and model drug stock solution were diluted in methanol. Then, the absorbance peaks of the dilute solutions were measured using UV-visible spectrophotometry. The characteristic peak of absorbance was determined at a wavelength of 499 nm. Eqs. (1) and (2) were used to calculate the encapsulation efficiencies and capacities, respectively.

$$\text{Encapsulation efficiency}\% = \frac{A_1 - A_2}{A_1} \times 100\% \quad (1)$$

$$\text{Encapsulation capacity wt.}\% = \frac{m_{\text{loaded}}}{m_{\text{loaded}} + m_{\text{MOF}}} \quad (2)$$

Where: A_1 = the absorbance of the model drug solution, A_2 = the absorbance of the supernatant, m_{loaded} = the mass of loaded model drug (mg), m_{MOF} = the mass of empty MOFs (mg).

Calcein Disodium Salt *In-Vitro* Release Experiments

The release of calcein disodium salt from loaded Fe-NDC nanoparticles was first studied without US triggering. We then investigated the effect of applying 40-kHz US at a power intensity of ~1 W/cm^2 (using a sonicating bath model DSC-50TH, Sonicor Inc., West Babylon, NY, USA) on release.

All the experiments were carried out at 37 °C a minimum of three times. Around 3 mg of dried calcein-loaded Fe-NDC particles were weighed, transferred into a plastic cuvette, and 3 ml of PBS were added. The absorbance was measured after 2, 4, 6, 8, and 10 min, and the release percentages were calculated using Eq. (3).

$$\text{CR}\% = \frac{A_t}{A_l} \quad (3)$$

where, CR% = The cumulative fractional release percentage, A_t = The absorbance at each time point, A_l = The absorbance of the loaded calcein disodium salt.

We first studied the release of the model drug from our MOFs over an extended period. Two of the loaded MOF samples were kept at 37 °C for an hour without applying an external stimulus. Then, the absorbance was quantified via UV-vis spectroscopy.

DOX Encapsulation and *In-Vitro* Release Experiments

DOX loading experiments were carried out in triplicates. For each run, 15 mg of Fe-NDC was mixed with 5 ml of a 3-mg/ml DOX solution in the dark at room temperature for 24 hours. Then, the resulting suspension was centrifuged for 1 hour at 4500 rpm (Heraeus Megafuge 8R, Thermo Scientific, Waltham, MA, USA), followed by decanting the supernatant and measuring the absorbance spectra to determine the final concentration of the DOX solution. Eqs. (1)

and (2) were used to calculate the encapsulation efficiency and capacity of Fe-NDC. The resulting nanoparticles were washed twice with deionized water and dried overnight to be used in the release experiments.

The experimental protocol for DOX release from loaded Fe-NDC was similar to that followed to release calcein from Fe-NDC. Briefly, 15 mg of the DOX-loaded Fe-NDC was added to 5 ml of a 0.01-M PBS solution at 37 °C. The experiments were carried out with and without exposure to US. For each run, 3 ml of PBS were taken after a specified time interval for spectral analysis and replaced with an equal amount of fresh PBS. Then the release percentage was calculated using Eq. (3).

Cell Studies

MCF-7 cells (ER-positive human breast adenocarcinoma (European Collection of Authenticated Cell Culture (ECACC))) were utilized in our *In-vitro* cell experiments. The cells were cultured in an RPMI medium, supplemented with 10% heat-inactivated FBS and 1% penicillin–streptomycin. The cell cultures were maintained in T-75 flasks at 37 °C in a humidified atmosphere incubator with 5.0% CO_2 until the cells were 80% confluent.

For the cytotoxicity tests, different amounts of as-synthesized Fe-NDC particles were dispersed in PBS via sonication to prepare solutions with concentrations of 12.5, 25, 50, 100, and 200 μg/ml. For the cytocompatibility analysis, the MCF-7 cells were harvested with trypsin and a cell density of 3×10^5 cell/ml of growth medium was seeded in 6-well plates. The cells were incubated overnight, allowing adherence to the wells.

Fresh media containing Fe-NDC solutions were introduced to the cells and incubated for 24 h. Then, the media were removed and the excess material washed off using PBS. The cells were trypsinized and quantitative analysis of toxicity was conducted by direct cell counting using a flow cytometer (Beckman Coulter FC500, Brea, CA, USA). Propidium Iodide was used to evaluate the % viability. All measurements were performed in triplicates of triplicates.

RESULTS AND DISCUSSION

Characterization of the Synthesized Fe-NDC

The nanoparticles have a rod-like shape (Fig. 1), as previously reported [53]. Several studies showed the higher uptake of poly-ethylene glycol hydrogel rods with dimensions of 150×450 nm compared to cylindrical particles of 200×200 nm, and trastuzumab-coated rods (367 ± 33 nm in length and 126 ± 8 nm in width) compared to 200-nm spheres, in different breast cancer cell lines. Thus, the rod shape of Fe-NDC may enhance the carriers' *In-vivo* cellular uptake compared to other spherical MOFs [58–60].

Figure 2 shows a type III physisorption isotherm. The adsorption average pore width was calculated to be ~9.3 nm using BET data. The XRD pattern of Fe-NDC

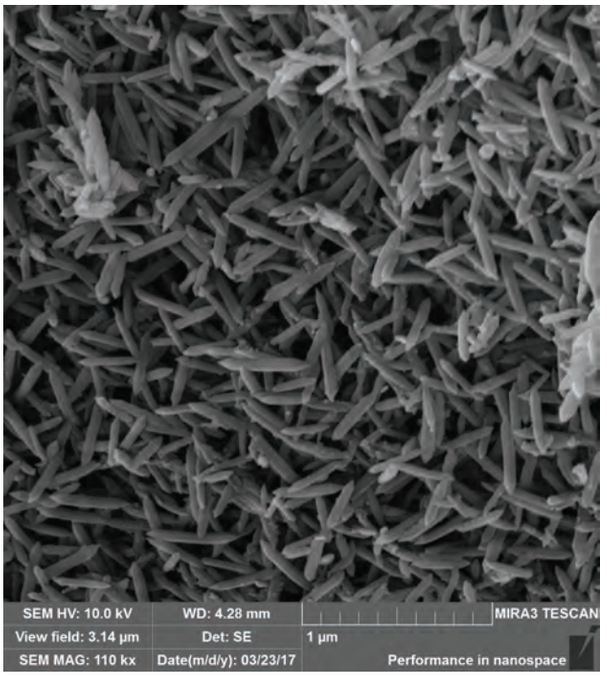

Figure 1. An SEM image of Fe-NDC showing the rod-like particle shape.

is illustrated in Figure 3. The XRD resemble a crystal structure of the prepared Fe-NDC MOF with distinguished 2θs of 7.5, 10.5, and 15, which match the earlier reported pattern [53]. In addition, the XRD patterns of the loaded MOFs showed that the crystallinity of the Fe-NDC particles was maintained, while the increased intensity of the distinct peaks at 2θ of 10.5 and 15 and the changes in the color of the MOF particles suggested the successful encapsulation of the target molecules (calcein and DOX) into the Fe-NDC framework. Furthermore, the similarity between the Fe-NDC-DOX and Fe-NDC-calcein XRD

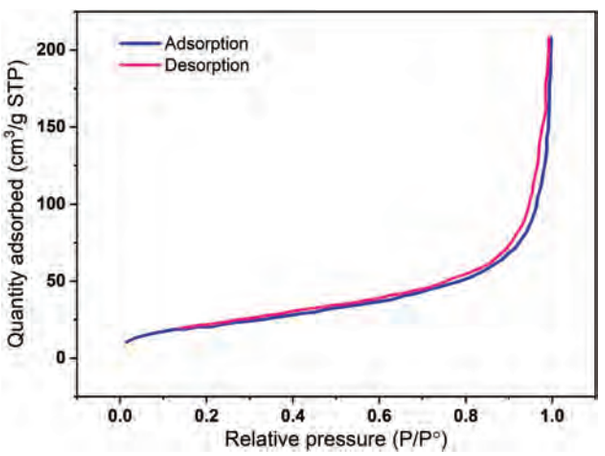

Figure 2. A nitrogen sorption isotherm of Fe-NDC, adsorption (blue)–desorption (red).

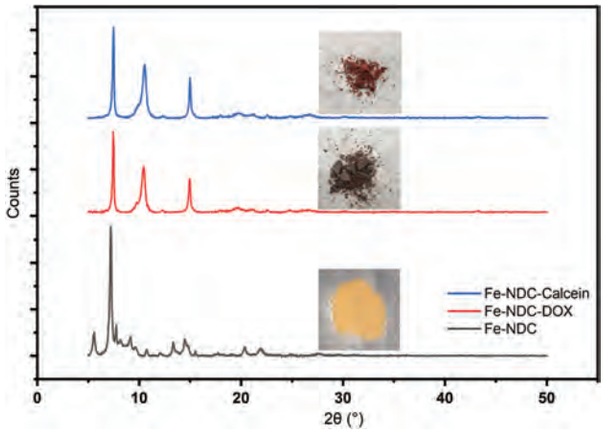

Figure 3. **The XRD patterns of Fe-NDC (black), Fe-NDC-DOX (red), and Fe-NDC-Calcein (blue) samples.**

patterns suggests the same encapsulation mechanisms of both molecules inside the MOF framework.

The particle size distribution of the synthesized Fe-NDC is shown in Figure 4. The results show that these nanoparticles had an average particle diameter of 230 nm, which is acceptable for drug delivery applications. The polydispersity index (PDI) is 0.14, indicating a moderately uniform particle size distribution. It should be noted that the particle diameter measured using the DLS technique is based on a spherical particle-shape assumption.

The Concentration of Calcein Disodium Salt

As seen in Figure 5, the absorbance peak increased as calcein's concentration increased. The calcein calibration curve was linear over the concentration range of 0.001 mM to 0.01 mM, generated using the first five concentrations, as shown in Figure 5. This curve was used to determine calcein's concentration to calculate the encapsulation and release percentages, as described in the following sections.

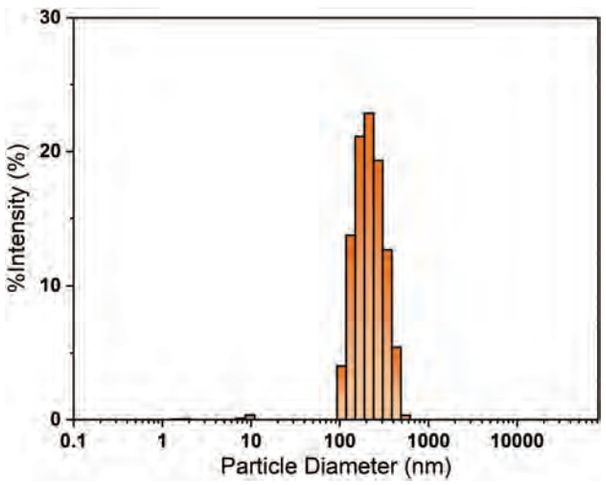

Figure 4. **The particle size distribution of Fe-NDC.**

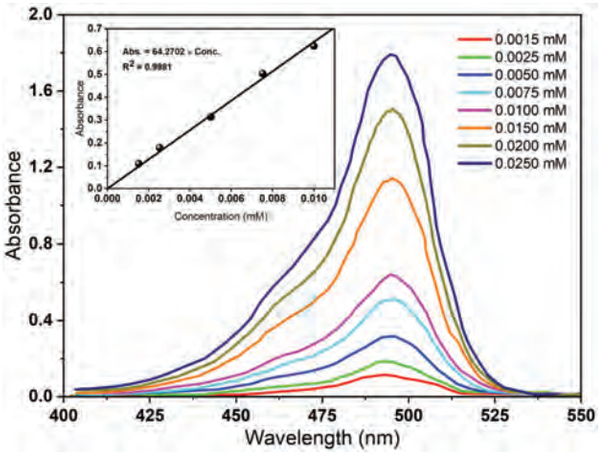

Figure 5. **The absorption spectra of calcein disodium salt solutions. The inset is the calibration curve for calcein disodium salt solutions.**

Calcein Encapsulation Efficiency and Capacity

The encapsulation mechanism of molecules in MOFs can be described simply by the guest molecules' adsorption onto the interior surface or inside the framework pores (See Fig. 6). Several forces govern this adsorbate–adsorbent interaction, including hydrogen bonds, hydrophobic (Van der Waals) forces, coordination bonds, or π–π interactions [24, 61, 62].

The absorbance peaks of the loaded calcein disodium salt onto Fe-NDC samples are shown in Figure 7. Based on these peaks, the encapsulation efficiencies were ~42.73, 43.77, and 42.91% for the first, second, and third runs, respectively, with an average of 43.13%. The encapsulation capacity based on the average efficiency was ~17.74 wt.%.

The MOF capacity was found to be slightly higher compared to Zr-L6 MOF, which showed a capacity of 15.2 wt.%. This percentage was considerably higher when the amorphous UiO-66 was used (4.9 ± 0.2 wt.%), which can be attributed to the relatively long organic linker used in synthesizing both Zr-L6 and Fe-NDC, resulting in larger pore volumes that enable the encapsulation of more molecules [63, 64].

Calcein *In-Vitro* Release Profiles Without and With Applying US

Calcein release profiles were explored at two different conditions: with and without external acoustic stimulus. As depicted in Figure 8, the average amount of calcein disodium salt released by diffusion from the MOF increased slightly with time to reach ~17.8% after 10 min without US. This slight premature leakage can be easily prevented by capping the MOF with carboxylate-pillar[5]arene-based supramolecular switches [65, 66], or coating its surface with sodium metasilicate, proteins, polymers, or lipid bilayers [67–69].

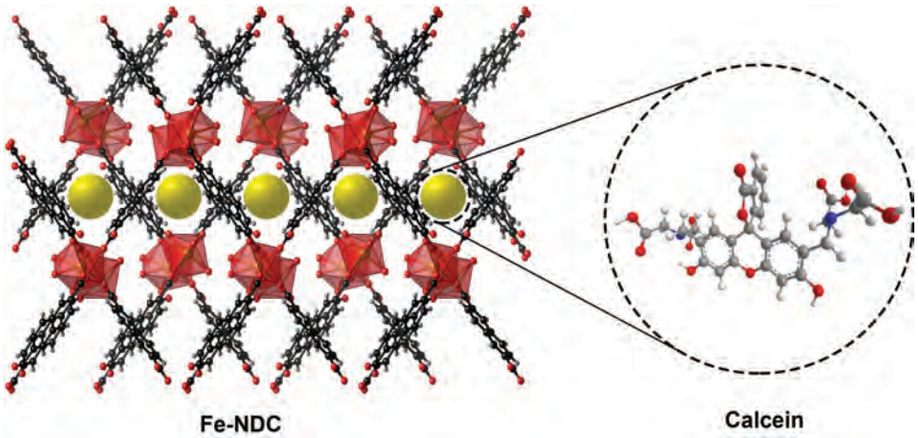

Figure 6. **A schematic illustrating the encapsulation of calcein molecules inside the framework pores of Fe-NDC. The yellow spheres represent the empty spaces inside the pores of the MOF.**

The release increased considerably when US was applied to reach ~95.2% (Fig. 8) (a 5.35-time higher release compared to samples not exposed to US). Since the temperature of the media hovered around 37 °C, this release may be attributed to the nonthermal (mechanical) effects of US. In particular, US waves cause the fluid medium to oscillate, producing mechanical stresses, which mixes the sample vigorously and results in the diffusion of calcein disodium salt from the MOF pores [70]. On the other hand, the samples left for an hour did not show further release compared to the amount released during the first 10 min (17.8% without US and 95.2% with US).

The results shown above confirmed the role of US in enhancing the oscillation of the Fe-NDC nanorods, which in turn triggered the release of the agent. Therefore, chemotherapeutic drugs loaded in MOFs can be delivered effectively, spatially and temporally, upon applying US at the tumor sites.

DOX Encapsulation and *In-Vitro* Release Profiles

Figure 9 presents the absorbance spectra of DOX solutions and the calibration curve used to quantify the amount of the chemotherapeutic agent in loading and release experiments. The absorbance spectra of the DOX loading solution and the supernatant are shown in Figure 10. Using this data, the average DOX encapsulation efficiency and capacity were determined to be 16.10% and 13.37 wt.%, respectively. DOX encapsulation in Fe-NDC can be attributed to the noncovalent and covalent interactions between the drug and the MOF. An example of the noncovalent interaction is the hydrogen bonding between DOX molecules and the 2,6-NDC ligand through donor–acceptor interactions (e.g., hydrogen-oxygen, and/or hydrogen-nitrogen) [24]. Another example of the noncovalent encapsulation mechanism is the π–π interactions between the benzene rings of the DOX molecules and the 2,6-NDC link-

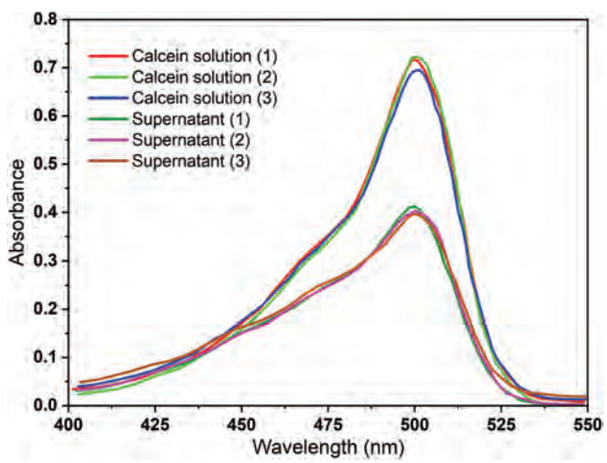

Figure 7. **Calcein UV-Vis spectra for the encapsulations.**

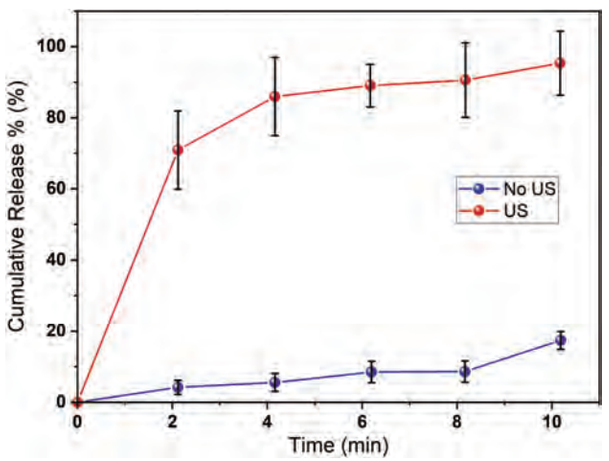

Figure 8. **Release profiles of calcein disodium salt from Fe-NDC without (blue) and with US (red). The error bars represent the standard deviation of the three replicates, while the points represent the average of these three independent replicates.**

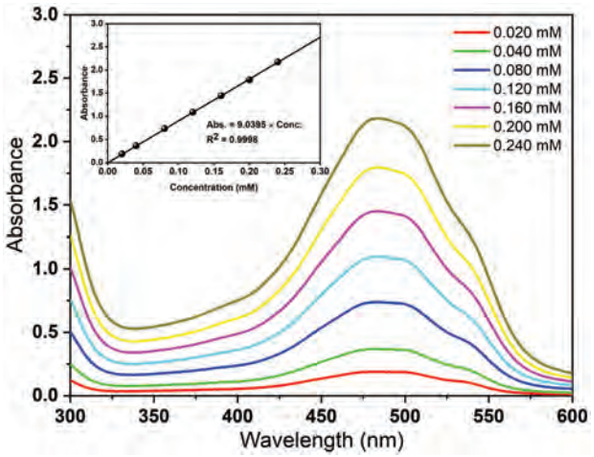

Figure 9. **Standard DOX solution absorbance spectra. Inset is the calibration curve.**

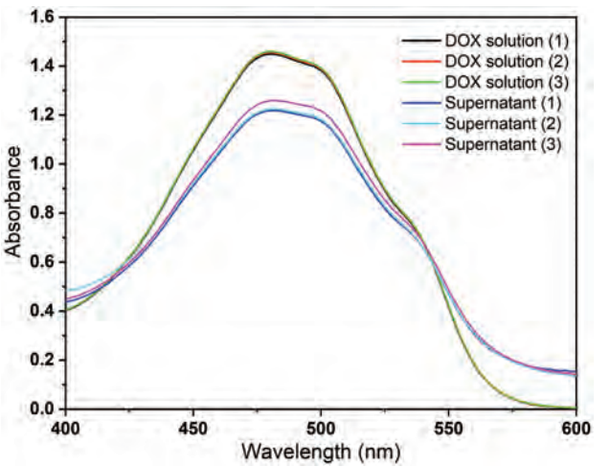

Figure 10. **Absorbance spectra of the DOX loading solution and supernatant.**

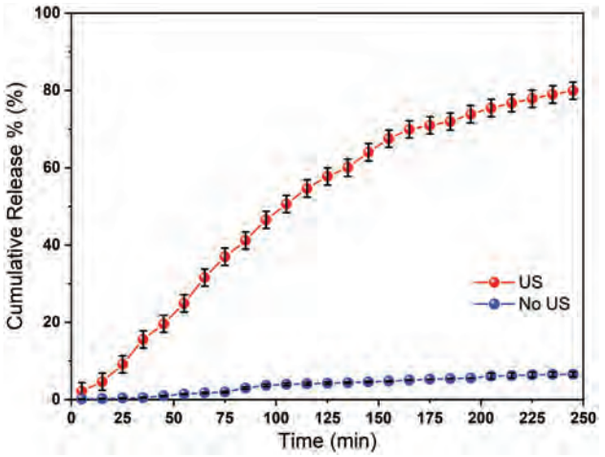

Figure 12. ***In-vitro*** **release profiles of DOX from Fe-NDC without US (blue) and with US (red). The error bars represent the standard deviation of the three replicates, while the points represent the average of these three independent replicates.**

ers [24]. DOX binding to Fe-NDC may also be possible through covalent interactions; by forming stable coordination bonds between DOX and the coordinately unsaturated iron atoms. Similar interactions have been reported for DOX encapsulation with other iron-based MOFs [27, 71, 72]. A schematic illustration of DOX loading in Fe-NDC is shown in Figure 11.

The *In-vitro* DOX release profiles (with and without US) are shown in Figure 12. The results reveal that the unassisted passive release of DOX was around 6% after 245 minutes, indicating the drug's low premature release. On the other hand, when US was applied, the release increased significantly, reaching 80% within the same time interval. This is attributed to the vigorous mixing and mechanical stresses on the loaded nanoparticles, which, in turn, enhanced the release of the drug from the MOFs structure. Table I presents a summary of DOX loading

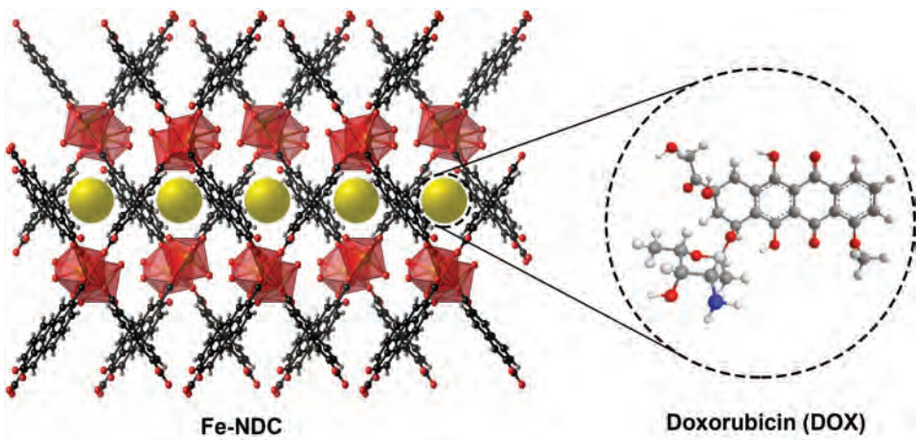

Figure 11. **The schematic illustration of DOX molecules encapsulated inside the framework pores of Fe-NDC. The yellow spheres represent the empty space inside the pores of the MOF.**

Table I. DOX loading capacities and release rates of various iron-based MOFs.

MOF nanocarrier	Stimulus	Loading capacity (wt.%)	Release rate (%)	Reference
MIL-100 (Fe)	–	9.1	100% after 13 days (PBS, pH 7.4)	[9]
Fe-BTC	–	6.5	69% after 16 days (PBS, pH 7.4)	[71]
MN@Fe-BTC	–	2.2	21% after 16 days (PBS, pH 7.4)	[71]
MIL-100 (Fe)	pH	28	66% after 60 hours (PBS, pH 5.5) 30% after 60 hours (PBS, pH 7.4)	[72]
$NaGdF_4$:Yb/Er@MIL-53 (Fe)/FA	pH	16	80% after 48 hours (PBS, pH 5.2) 67.5% after 48 hours (PBS, pH 7.4)	[73]
Fe-NDC	– Ultrasound	13.37 13.37	6% after 245 minutes (PBS, pH 7.4) 80% after 245 minutes (PBS, pH 7.4)	This work

efficiencies and stimuli-responsive release rates of various iron-based MOFs. The table shows that the encapsulation capacity of Fe-NDC is comparable with that of other iron-based MOFs. Furthermore, the use of US as a stimulus gave a higher DOX release rate compared to the other iron-based MOFs.

In-Vitro Cytotoxicity Analysis of Fe-NDC

The effect of Fe-NDC-M on cell viability is shown in Figure 13. MOF concentrations of 12.5, 25, 50, 100, and 200 μg/ml resulted in viabilities of 95.95%, 94.03%, 93.95%, 90.77%, and 85.11%, respectively. In addition, the Graphpad Prism software was used to estimate the half-maximal inhibitory concentration (IC_{50}) of MOFs towards MCF-7 cells, which was calculated to be 1022 μg/ml.

Figure 13 shows that Fe-NDC MOFs are biocompatible even at relatively higher concentrations. Also, the IC_{50} is moderate and comparable to other MOFs, indicating the potential use of Fe-NDC nanorods in various biomedical applications, especially for site-specific anticancer drug delivery.

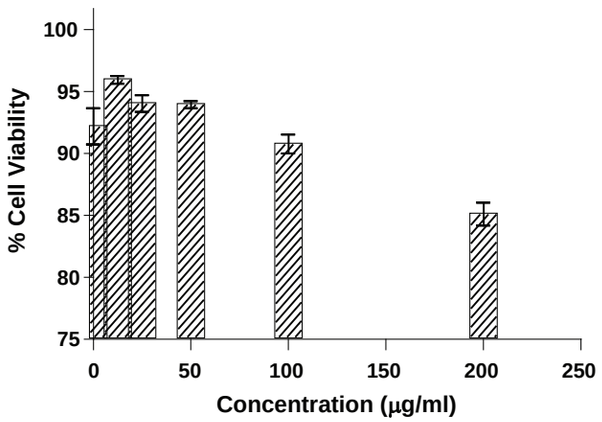

Figure 13. Flow cytometric evaluation of % viability at different concentrations of MOF in μg/ml after 24 h of incubation.

CONCLUSIONS

In this research paper, we reported the first use of iron and 2,6-naphthalene dicarboxylic acid-based MOF (Fe-NDC) nanorods, as nanocarriers to encapsulate calcein disodium salt (fluorescent model drug) and DOX (a topoisomerase inhibitor). SEM images showed that our MOF nanoparticles had a rod-like shape, while the XRD patterns showed that Fe-NDC had a crystalline structure. The XRD patterns of calcein- and DOX-loaded Fe-NDC samples suggested that the MOFs maintained their crystallinity and that the DOX encapsulation mechanism is similar to that of calcein's. The average pore width was calculated to be ~9.3 nm using BET analysis. The average particle diameter from DLS analysis was 230 nm, based on a spherical particle-shape assumption. Calcein's loading and *In-vitro* release experiments showed that the average encapsulation efficiency and capacity were ~43.13% and 17.74 wt.%, respectively. Within 10 min, the encapsulated model drug/dye was released slowly (17.8%) without an external stimulus. In contrast, the nanocarriers exhibited rapid and substantial release (95.2%) when low-frequency ultrasound (LFUS) was applied. The average DOX encapsulation efficiency and capacity were determined to be 16.10% and 13.37 wt.%, respectively. *In-vitro* DOX release experiments demonstrated an enhanced release rate (80% in 245 minutes) under simulated physiological conditions (PBS, pH 7.4 at 37 °C) when US was applied, while the unassisted passive (without US) release was around 6% during the same time interval. Finally, *In-vitro* cytotoxicity experiments of Fe-NDC against MCF7 cells showed high biocompatibility in the concentration range evaluated (up to 200 μg/ml). All of these findings confirm (1) the potential use of Fe-NDC as a candidate for encapsulating high amounts of antineoplastic agents and (2) US as a trigger mechanism to release the therapeutic cargo at the diseased location.

Acknowledgment: The authors gratefully acknowledge the financial support by the American University of Sharjah Enhanced Faculty Research Grant EFRG18-BBR-CEN-03.

REFERENCES

1. Svenson, S., **2012**. Clinical translation of nanomedicines. *Current Opinion in Solid State and Materials Science*, *16*(6), pp.287–294.
2. Markman, J.L., Rekechenetskiy, A., Holler, E. and Ljubimova, J.Y., **2013**. Nanomedicine therapeutic approaches to overcome cancer drug resistance. *Advanced Drug Delivery Reviews*, *65*(13–14), pp.1866–1879.
3. Wang, X., Li, S., Shi, Y., Chuan, X., Li, J., Zhong, T., Zhang, H., Dai, W., He, B. and Zhang, Q., **2014**. The development of site-specific drug delivery nanocarriers based on receptor mediation. *Journal of Controlled Release*, *193*, pp.139–153.
4. Hou, D., Gui, R., Hu, S., Huang, Y., Feng, Z.F. and Ping, Q., **2015**. Preparation and characterization of novel drug-inserted-montmorillonite chitosan carriers for ocular drug delivery. *Advances in Nanoparticles*, *4*(3), pp.70–84.
5. Kanapathipillai, M., Brock, A. and Ingber, D.E., **2014**. Nanoparticle targeting of anticancer drugs that alter intracellular signaling or influence the tumor microenvironment. *Advanced Drug Delivery Reviews*, *79–80*, pp.107–118.
6. Ibrahim, M., Sabouni, R. and Husseini, G., **2017**. Anticancer drug delivery using metal organic frameworks (MOFs). *Current Medicinal Chemistry*, *24*(2), pp.193–214.
7. Keskin, S. and Kızılel, S., **2011**. Biomedical applications of metal organic frameworks. *Industrial & Engineering Chemistry Research*, *50*(4), pp.1799–1812.
8. Huxford, R.C., Della Rocca, J. and Lin, W., **2010**. Metal-organic frameworks as potential drug carriers. *Current Opinion in Chemical Biology*, *14*(2), pp.262–268.
9. Horcajada, P., Chalati, T., Serre, C., Gillet, B., Sebrie, C., Baati, T., Eubank, J.F., Heurtaux, D., Clayette, P., Kreuz, C., Chang, J.-S., Hwang, Y.K., Marsaud, V., Bories, P.-N., Cynober, L., Gil, S., Férey, G., Couvreur, P. and Gref, R., **2010**. Porous metal-organic-framework nanoscale carriers as a potential platform for drug delivery and imaging. *Nature Materials*, *9*(2), pp.172–178.
10. Danhier, F., Feron, O. and Préat, V., **2010**. To exploit the tumor microenvironment: Passive and active tumor targeting of nanocarriers for anticancer drug delivery. *Journal of Controlled Release*, *48*(2), pp.135–146.
11. Torchilin, V.P., **2007**. Targeted pharmaceutical nanocarriers for cancer therapy and imaging. *The AAPS Journal*, *9*(2), pp.E128–E147.
12. Graf, N. and Lippard, S.J., **2012**. Redox activation of metal-based prodrugs as a strategy for drug delivery. *Advanced Drug Delivery Reviews*, *64*(11), pp.993–1004.
13. Matsumura, Y. and Maeda, H., **1986**. A new concept for macromolecular therapeutics in cancer chemotherapy: Mechanism of tumoritropic accumulation of proteins and the antitumor agent smancs. *Cancer Research*, *46*(12), pp.6387–6392.
14. Hobbs, S.K., Monsky, W.L., Yuan, F., Roberts, W.G., Griffith, L., Torchilin, V.P. and Jain, R.K., **1998**. Regulation of transport pathways in tumor vessels: Role of tumor type and microenvironment. *Proceedings of the National Academy of Sciences*, *5*(8), pp.4607–4612.
15. Jiang, J.X., Keating, J.J., Jesus, E.M.D., Judy, R.P., Madajewski, B., Venegas, O., Okusanya, O.T. and Singhal, S., **2015**. Optimization of the enhanced permeability and retention effect for near-infrared imaging of solid tumors with indocyanine green. *American Journal of Nuclear Medicine and Molecular Imaging*, *5*(4), pp.390–400.
16. Bertrand, N., Wu, J., Xu, X., Kamaly, N. and Farokhzad, O.C., **2014**. Cancer nanotechnology: The impact of passive and active targeting in the era of modern cancer biology. *Advanced Drug Delivery Reviews*, *66*, pp.2–25.
17. Díaz, M. and Vivas-Mejia, P., **2013**. Nanoparticles as drug delivery systems in cancer medicine: Emphasis on RNAi-containing nanoliposomes. *Pharmaceuticals*, *6*(11), pp.1361–1380.
18. Chen, Y., Chen, H. and Shi, J., **2014**. Inorganic nanoparticle-based drug codelivery nanosystems to overcome the multidrug resistance of cancer cells. *Molecular Pharmaceutics*, *11*(8), pp.2495–2510.
19. Lee, J.J., Yazan, L.S. and Abdullah, C.A., **2017**. A review on current nanomaterials and their drug conjugate for targeted breast cancer treatment. *International Journal of Nanomedicine*, *12*, pp.2373–2384.
20. Kuppler, R.J., Timmonsb, D.J., Fang, Q.-R., Li, J.-R., Makal, T.A., Young, M.D., Yuan, D., Zhao, D., Zhuang, W. and Zhou, H.-C., **2009**. Potential applications of metal-organic frameworks. *Coordination Chemistry Reviews*, *253*(23–24), pp.3042–3066.
21. Cai, W., Chu, C., Liu, G. and Wáng, G.L.J., **2015**. Metal-organic framework-based nanomedicine platforms for drug delivery and molecular imaging. *Small*, *11*(37), pp.1–17.
22. McKinlay, A.C., Morris, R.E., Horcajada, P., Férey, G., Gref, R., Couvreur, P. and Serre, C., **2010**. BioMOFs: Metal-organic frameworks for biological and medical applications. *Angewandte Chemie International Edition*, *49*, pp.6260–6266.
23. Wang, C., Liu, D. and Lin, W., **2013**. Metal-organic frameworks as a tunable platform for designing functional molecular materials. *Journal of the American Chemical Society*, *135*(36), pp.13222–13234.
24. Horcajada, P., Gref, R., Baati, T., Allan, P. K., Maurin, G., Couvreur, P., Férey, G., Morris, R.E. and Serre, C., **2012**. Metal-organic frameworks in biomedicine. *Chemical Reviews*, *112*(2), pp.1232–1268.
25. Horcajada, P., Serre, C., Maurin, G., Ramsahye, N. A., Balas, F., Vallet-Regí, M.,…Férey, G., **2008**. Flexible porous metal-organic frameworks for a controlled drug delivery. *Journal of the American Chemical Society*, *130*(21), pp.6774–6780.
26. Chalati, T., Horcajada, P., Couvreur, P., Serre, C., Yahia, M.B., Maurin, G. and Gref, R., **2011**. Porous metal-organic framework nanoparticles to address the challenges related to busulfan encapsulation. *Nanomedicine*, *6*(10), pp.1683–1695.
27. Anand, R., Borghi, F., Manoli, F., Manet, I., Agostoni, V., Reschiglian, P., Gref, R. and Monti, S., **2014**. Host–guest interactions in Fe(III)-trimesate MOF nanoparticles loaded with doxorubicin. *The Journal of Physical Chemistry B*, *118*(29), pp.8532–8539.
28. di Nunzio, M.R., Agostoni, V., Cohen, B., Gref, R. and Douhal, A., **2014**. A "ship in a bottle" strategy to load a hydrophilic anticancer drug in porous metal organic framework nanoparticles: Efficient encapsulation, matrix stabilization, and photodelivery. *Journal of Medicinal Chemistry*, *57*(2), pp.411–420.
29. Zhuang, J., Kuo, C.-H., Chou, L.-Y., Liu, D.-Y., Weerapana, E. and Tsung, C.-K., **2014**. Optimized metal-organic framework nanospheres for drug delivery: Evaluation of small-molecule encapsulation. *ACS Nano*, *8*(3), pp.2812–2819.
30. Zheng, H., Zhang, Y., Liu, L., Wan, W., Guo, P., Nyström, A.M. and Zou, X., **2016**. One-pot synthesis of metal-organic frameworks with encapsulated target molecules and their applications for controlled drug delivery. *Journal of the American Chemical Society*, *138*(3), pp.962–968.
31. Sun, C.-Y., Qin, C., Wang, X.-L., Yang, G.-S., Shao, K.-Z., Lan, Y.-Q., Su, Z.-M., Huang, P., Wang, C.-G. and Wang, E.-B., **2012**. Zeolitic imidazolate framework-8 as efficient pH-sensitive drug delivery vehicle. *Dalton Transactions*, *41*(23), pp.6906–6909.
32. García Márquez, A., Demessence, A., Platero-Prats, A.E., Heurtaux, D., Horcajada, P., Serre, C., Chang, J.-S., Férey, G., de la Peña-O'Shea, V.A., Boissière, C., Grosso, D. and Sanchez, C., **2012**. Green microwave synthesis of MIL-100(Al, Cr, Fe) nanoparticles for thin-film elaboration. *European Journal of Inorganic Chemistry*, *2012*(32), pp.5165–5174.
33. Rojas, S., Carmona, F.J., Maldonado, C.R., Horcajada, P., Hidalgo, T., Serre, C., Navarro, J.A.R. and Barea, E., **2016**. Nanoscaled zinc pyrazolate metal-organic frameworks as drug-delivery systems. *Inorganic Chemistry*, *55*(5), pp.2650–2663.

34. Husseini, G.A. and Pitt, W.G., **2008**. Micelles and nanoparticles for ultrasonic drug and gene delivery. *Advanced Drug Delivery Reviews*, *60*(10), pp.1137–1152.

35. Ganta, S., Devalapally, H., Shahiwala, A. and Amiji, M., **2008**. A review of stimuli-responsive nanocarriers for drug and gene delivery. *Journal of Controlled Release*, *126*(3), pp.187–204.

36. Zhou, Q.-L., Chen, Z.-Y., Wang, Y.-X., Yang, F., Lin, Y. and Liao, Y.-Y., **2014**. Ultrasound-mediated local drug and gene delivery using nanocarriers. *BioMed Research International*, *2014*, pp.1–13.

37. Mishra, B., Patel, B.B. and Tiwari, S., **2010**. Colloidal nanocarriers: A review on formulation technology, types and applications toward targeted drug delivery. *Nanomedicine*, *6*(1), pp.9–24.

38. Husseini, G.A., Myrup, G.D., Pitt, W.G., Christensen, D.A. and Rapoport, N.Y., **2000**. Factors affecting acoustically triggered release of drugs from polymeric micelles. *Journal of Controlled Release*, *69*(1), pp.43–52.

39. Mura, S., Nicolas, J. and Couvreur, P., **2013**. Stimuli-responsive nanocarriers for drug delivery. *Nature Materials*, *12*(11), pp.991–1003.

40. Udroiu, I., **2015**. Ultrasonic drug delivery in Oncology. *JBUON*, *20*(2), pp.381–390.

41. Lim, E.-K., Jang, E., Lee, K., Haam, S. and Huh, Y.-M., **2013**. Delivery of cancer therapeutics using nanotechnology. *Pharmaceutics*, *5*(2), pp.294–317.

42. Baker, K.G., Robertson, V.J. and Duck, F.A., **2001**. A review of therapeutic ultrasound: Biophysical effects. *Physical Therapy*, *81*(7), pp.1351–1358.

43. Mitragotri, S., **2005**. Healing sound: The use of ultrasound in drug delivery and other therapeutic applications. *Nature Reviews Drug Discovery*, *4*(3), pp.255–260.

44. Park, D., Park, H., Seo, J. and Lee, S., **2014**. Sonophoresis in transdermal drug deliverys. *Ultrasonics*, *54*(1), pp.56–65.

45. Takahashi, H., **2005**. Free radical development in phacoemulsification cataract surgery. *Journal of Nippon Medical School*, *72*(1), pp.4–12.

46. Cooter, R., Babidge, W., Mutimer, K., Wickham, P., Robinson, D., Kiroff, G., Chapman, A. and Maddern, G., **2001**. Ultrasound-assisted lipoplasty. *ANZ Journal of Surgery*, *71*(5), pp.309–317.

47. Siegel, R.J. and Luo, H., **2008**. Ultrasound thrombolysis. *Ultrasonics*, *48*(4), pp.312–320.

48. Miller, D., **2007**. Overview of experimental studies of biological effects of medical ultrasound caused by gas body activation and inertial cavitation. *Progress in Biophysics and Molecular Biology*, *93*(1–3), pp.314–330.

49. Miller, D.L., Smith, N.B., Bailey, M.R., Czarnota, G.J., Hynynen, K. and Makin, I.R.S., **2012**. Overview of therapeutic ultrasound applications and safety considerations. *Journal of Ultrasound in Medicine*, *31*(4), pp.623–634.

50. Ahmadi, F., McLoughlin, I.V., Chauhan, S. and Ter-Haar, G., **2012**. Bio-effects and safety of low-intensity, low-frequency ultrasonic exposure. *Progress in Biophysics and Molecular Biology*, *108*(3), pp.119–138.

51. Izadifar, Z., Babyn, P. and Chapman, D., **2017**. Mechanical and biological effects of ultrasound: A review of present knowledge. *Ultrasound in Medicine & Biology*, *43*(6), pp.1085–1104.

52. Pasquinelli, C., Hanson, L.G., Siebner, H.R., Lee, H.J. and Thielscher, A., **2019**. Safety of transcranial focused ultrasound stimulation: A systematic review of the state of knowledge from both human and animal studies. *Brain Stimulation*, *12*(6), pp.1367–1380.

53. Ibrahim, M., Sabouni, R. and Husseini, G., **2018**. Synthesis of metal-organic framework from iron nitrate and 2,6-naphthalenedicarboxylic acid and its application as drug carrier. *Journal of Nanoscience and Nanotechnology*, *18*(8), pp.5266–5273.

54. Hamann, S., Kiilgaard, J.F., Litman, T., Alvarez-Leefmans, F.J., Winther, B.R. and Zeuthen, T., **2002**. Measurement of cell volume changes by fluorescence self-quenching. *Journal of Fluorescence*, *12*(2), pp.139–145.

55. Zhang, X., Luckham, P.F., Hughes, A.D., Thom, S. and Xu, X.Y., **2013**. Towards an understanding of the release behavior of temperature-sensitive liposomes: A possible explanation of the "pseudoequilibrium" release behavior at the phase transition temperature. *Journal of Liposome Research*, *23*(3), pp.167–173.

56. Javadi, M., Pitt, W.G., Tracy, C.M., Barrow, J.R., Willardson, B.M., Hartley, J.M. and Tsosie, N.H., **2013**. Ultrasonic gene and drug delivery using eLiposomes. *Journal of Controlled Release*, *167*(1), pp.92–100.

57. Gratton, S.E.A., Ropp, P.A., Pohlhaus, P.D., Luft, J.C., Madden, V.J., Napier, M.E. and DeSimone, J.M., **2008**. The effect of particle design on cellular internalization pathways. *Proceedings of the National Academy of Sciences*, *105*(33), pp.11613–11618.

58. Barua, S., Yoo, J.-W., Kolhar, P., Wakankar, A., Gokarn, Y.R. and Mitragotri, S., **2013**. Particle shape enhances specificity of antibody-displaying nanoparticles. *Proceedings of the National Academy of Sciences*, *110*(9), pp.3270–3275.

59. Zhu, M., Nie, G., Meng, H., Xia, T., Nel, A. and Zhao, Y., **2013**. Physicochemical properties determine nanomaterial cellular uptake, transport, and fate. *Accounts of Chemical Research*, *46*(3), pp.622–631.

60. Cunha, D., Ben Yahia, M., Hall, S., Miller, S.R., Chevreau, H., Elkaïm, E., Maurin, G., Horcajada, P. and Serre, C., **2013**. Rationale of drug encapsulation and release from biocompatible porous metal-organic frameworks. *Chemistry of Materials*, *25*(14), pp.2767–2776.

61. Hu, Q., Yu, J., Liu, M., Liu, A., Dou, Z. and Yang, Y., **2014**. A low cytotoxic cationic metal-organic framework carrier for controllable drug release. *Journal of Medicinal Chemistry*, *57*(13), pp.5679–5685.

62. Orellana-Tavra, C., Baxter, E.F., Tian, T., Bennett, T.D., Slater, N.K.H., Cheetham, A.K. and Fairen-Jimenez, D., **2015**. Amorphous metal-organic frameworks for drug delivery. *Chemical Communications*, *51*(73), pp.13878–13881.

63. Orellana-Tavra, C., Marshall, R.J., Baxter, E.F., Lázaro, I.A., Tao, A., Cheetham, A.K., Forgan, R.S. and Fairen-Jimenez, D., **2016**. Drug delivery and controlled release from biocompatible metal-organic frameworks using mechanical amorphization. *Journal of Materials Chemistry B*, *4*(47), pp.7697–7707.

64. Tan, L.-L., Li, H., Zhou, Y., Zhang, Y., Feng, X., Wang, B. and Yang, Y.-W., **2015**. Zn^{2+}-triggered drug release from biocompatible zirconium MOFs equipped with supramolecular gates. *Small*, *11*(31), pp.3807–3813.

65. Tan, L.-L., Song, N., Zhang, S. X.-A., Li, H., Wang, B. and Yang, Y.-W., **2016**. Ca^{2+}, pH and thermo triple-responsive mechanized Zr-based MOFs for on-command drug release in bone diseases. *Journal of Materials Chemistry B*, *4*(1), pp.135–140.

66. Taylor-Pashow, K.M.L., Della Rocca, J., Xie, Z., Tran, S. and Lin, W., **2009**. Postsynthetic modifications of iron-carboxylate nanoscale metal-organic frameworks for imaging and drug delivery. *Journal of the American Chemical Society*, *131*(40), pp.14261–14263.

67. Illes, B., Hirschle, P., Barnert, S., Cauda, V., Wuttke, S. and Engelke, H., **2017**. Exosome-coated metal-organic framework nanoparticles: An efficient drug delivery platform. *Chemistry of Materials*, *29*(19), pp.8042–8046.

68. Illes, B., Wuttke, S. and Engelke, H., **2017**. Liposome-coated iron fumarate metal-organic framework nanoparticles for combination therapy. *Nanomaterials*, *7*(11), p.351.

69. Canavese, G., Ancona, A., Racca, L., Canta, M., Dumontel, B., Barbaresco, F., Limongi T. and Cauda, V., **2018**. Nanoparticle-assisted ultrasound: A special focus on sonodynamic therapy against cancer. *Chemical Engineering Journal*, *340*, pp.155–172.

70. Tamames-Tabar, C., Cunha, D., Imbuluzqueta, E., Ragon, F., Serre, C., Blanco-Prieto, M.J. and Horcajada, P., **2014**. Cytotoxicity of nanoscaled metal-organic frameworks. *Journal of Materials Chemistry B*, *2*(3), pp.262–271.

71. Bellusci, M., Guglielmi, P., Masi, A., Padella, F., Singh, G., Yaacoub, N., Peddis, D. and Secci, D., **2018**. Magnetic metal-organic framework composite by fast and facile mechanochemical process. *Inorganic Chemistry*, *57*(4), pp.1806–1814.

72. Xue, T., Xu, C., Wang, Y., Wang, Y., Tian, H. and Zhang, Y., **2019**. Doxorubicin-loaded nanoscale metal-organic framework for tumor-targeting combined chemotherapy and chemodynamic therapy. *Biomaterials Science*, *7*(11), pp.4615–4623.

73. Mukherjee, P., Kumar, A., Bhamidipati, K., Puvvada, N. and Sahu, S.K., **2020**. Facile strategy to synthesize magnetic upconversion nanoscale metal-organic framework composites for theranostics application. *ACS Applied Bio Materials*, *3*(2), pp.869–880.